J|A|C|S ARTICLES

Published on Web 09/14/2010

Linker-Directed Vertex Desymmetrization for the Production of Coordination Polymers with High Porosity

Jennifer K. Schnobrich,[†] Olivier Lebel,[†,§] Katie A. Cychosz,[†] Anne Dailly,[‡] Antek G. Wong-Foy,[†] and Adam J. Matzger*[,†]

Department of Chemistry and Macromolecular Science and Engineering Program, University of Michigan, 930 North University Avenue, Ann Arbor, Michigan, 48109-1055, Chemical Sciences and Materials Systems Laboratory, General Motors, Warren, Michigan 48090

Received August 17, 2010; E-mail: matzger@umich.edu

Abstract: Five non-interpenetrated microporous coordination polymers (MCPs) are derived by vertex desymmetrization using linkers with symmetry inequivalent coordinating groups, and these MCPs include properties such as rare metal clusters, new network topologies, and supramolecular isomerism. Gas sorption in polymorphic frameworks, UMCM-152 and UMCM-153 (based upon a copper-coordinated tetracarboxylated triphenylbenzene linker), reveals nearly identical properties with BET surface areas in the range of 3300−3500 m^2/g and excess hydrogen uptake of 5.7 and 5.8 wt % at 77 K. In contrast, adsorption of organosulfur compounds dibenzothiophene (DBT) and 4,6-dimethyldibenzothiophene (DMDBT) shows remarkably different capacities, providing direct evidence that liquid-phase adsorption is not solely dependent on surface area or linker/metal cluster identity. Structural features present in MCPs derived from these reduced symmetry linkers include the presence of more than one type of Cu-paddlewheel in a structure derived from a terphenyl tricarboxylate (UMCM-151) and a three-bladed zinc paddlewheel metal cluster in an MCP derived from a pentacarboxylated triphenylbenzene linker (UMCM-154).

Introduction

A revolution in the production of new porous materials has come in the past decade due to the development of crystalline microporous coordination polymers (MCPs) as a potentially viable alternative to traditional zeolite and carbonaceous sorbents. Surface areas exceeding 3000 m^2/g have been reported for numerous MCPs[1−15] and values exceeding 5000 m^2/g are now obtainable.[4,14,15] This has been achieved almost exclusively using the traditional paradigm of a single symmetrical linker joined by a single metal cluster. Recently the potential of reduced symmetry linkers has been demonstrated; having one type of coordinating group in different chemical environments offers the potential to expose new regions of phase space, ultimately enabling the discovery of novel materials.[16−20]

Inspiration for reduced symmetry linkers is derived from the strategy of linker extension. Symmetrical linker extension has been established as a general method for the synthesis of new MCPs, with some materials having the same network topology as their unextended frameworks and others forming entirely new structures. However, this strategy can be limiting due to the tendency of larger linkers to form structures that interpenetrate or collapse upon guest removal. By removing the constraint of retaining a fully symmetric linker, two conceptual pathways for

[†] University of Michigan.
[§] Current address: Department of Chemistry and Chemical Engineering, Royal Military College of Canada, Kingston, Ontario, Canada K7K 7B4.
[‡] General Motors.

(1) Wong-Foy, A. G.; Matzger, A. J.; Yaghi, O. M. *J. Am. Chem. Soc.* **2006**, *128*, 3494–3495.
(2) Kaye, S. S.; Dailly, A.; Yaghi, O. M.; Long, J. R. *J. Am. Chem. Soc.* **2007**, *129*, 14176–14177.
(3) Koh, K.; Wong-Foy, A. G.; Matzger, A. J. *Angew. Chem., Int. Ed.* **2008**, *47*, 677–680.
(4) Koh, K.; Wong-Foy, A. G.; Matzger, A. J. *J. Am. Chem. Soc.* **2009**, *131*, 4184–4185.
(5) Porter, W. W.; Wong-Foy, A.; Dailly, A.; Matzger, A. J. *J. Mater. Chem.* **2009**, *19*, 6489–6491.
(6) Sumida, K.; Hill, M. R.; Horike, S.; Dailly, A.; Long, J. R. *J. Am. Chem. Soc.* **2009**, *131*, 15120–15121.
(7) Yan, Y.; Lin, X.; Yang, S. H.; Blake, A. J.; Dailly, A.; Champness, N. R.; Hubberstey, P.; Schröder, M. *Chem. Commun.* **2009**, 1025–1027.
(8) Wang, X.-S.; Ma, S.; Yuan, D.; Yoon, J. W.; Hwang, Y. K.; Chang, J.-S.; Wang, X.; Jørgensen, M. R.; Chen, Y.-S.; Zhou, H.-C. *Inorg. Chem.* **2009**, *48*, 7519–7521.
(9) Zhao, D.; Yuan, D.; Sun, D.; Zhou, H.-C. *J. Am. Chem. Soc.* **2009**, *131*, 9186–9188.
(10) Férey, G.; Mellot-Draznieks, C.; Serre, C.; Millange, F.; Dutour, J.; Surble, S.; Margiolaki, I. *Science* **2005**, *309*, 2040–2042.
(11) Hong, S.; Oh, M.; Park, M.; Yoon, J. W.; Chang, J.-S.; Lah, M. S. *Chem. Commun.* **2009**, 5397–5399.
(12) Yan, Y.; Telepeni, I.; Yang, S.; Lin, X.; Kockelmann, W.; Dailly, A.; Blake, A. J.; Lewis, W.; Walker, G. S.; Allan, D. R.; Barnett, S. A.; Champness, N. R.; Schröder, M. *J. Am. Chem. Soc.* **2010**, *132*, 4092–4094.
(13) Ma, S. Q.; Sun, D. F.; Ambrogio, M.; Fillinger, J. A.; Parkin, S.; Zhou, H. C. *J. Am. Chem. Soc.* **2007**, *129*, 1858–1859.
(14) Furukawa, H.; Ko, N.; Go, Y. B.; Aratani, N.; Choi, S. B.; Choi, E.; Yazaydin, A. O.; Snurr, R. Q.; O'Keeffe, M.; Kim, J.; Yaghi, O. M. *Science* **2010**, *239*, 424–428.
(15) Yuan, D.; Zhao, D.; Sun, D.; Zhou, H.-C. *Angew. Chem., Int. Ed.* **2010**, *49*, 5357–5361.
(16) Wong-Foy, A. G.; Lebel, O.; Matzger, A. J. *J. Am. Chem. Soc.* **2007**, *129*, 15740–15741.
(17) Feng, L.; Chen, Z. X.; Liao, T. B.; Li, P.; Jia, Y.; Liu, X. F.; Yang, Y. T.; Zhou, Y. M. *Cryst. Growth Des.* **2009**, *9*, 1505–1510.
(18) Guo, Z.; Li, G.; Zhou, L.; Su, S.; Lei, Y.; Dang, S.; Zhang, H. *Inorg. Chem.* **2009**, *48*, 8069–8071.
(19) Ma, L. Q.; Lin, W. B. *Angew. Chem., Int. Ed.* **2009**, *48*, 3637–3640.
(20) Ma, L. Q.; Mihalcik, D. J.; Lin, W. B. *J. Am. Chem. Soc.* **2009**, *131*, 4610–4612.

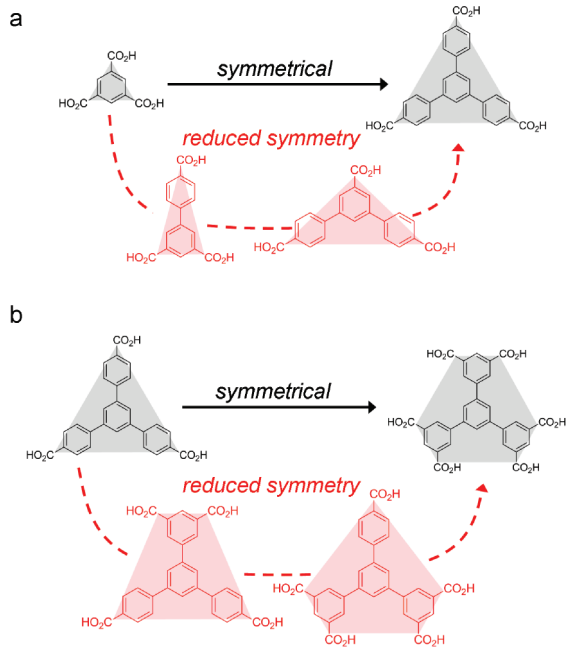

Figure 1. Conceptual modification of linkers through (a) ring and (b) carboxylate addition.

the production of new linkers can be envisaged: ring addition, in which the shape of a linker is only partially extended, and carboxylate addition/rearrangement, where the size and core connectivity of the linker remains unchanged but the addition and/or rearrangement of carboxylate groups produces more than one symmetry inequivalent coordinating group (Figure 1). Both methods introduce new types of building blocks and therefore expand the library of linkers available for coordination to a metal for the formation of new MCPs.

A potential benefit of using reduced symmetry linkers is the suppression of framework interpenetration. Because the growth of one framework into another reduces internal space that could otherwise be available to guests, interpenetration control is an important challenge in the synthesis of new materials. Recent efforts in this area have focused on liquid-phase epitaxial growth,[21] incorporation of steric bulk on the linker[22] or coordinating guests,[23] adjustments in solution concentration and reaction temperature,[24] and the use of templating agents.[13] Yet another approach is to use highly symmetric linkers that are geometrically predisposed to avoid interpenetration.[7,9,12,15,25,26] In considering general routes to porous solids, the tendency of many building blocks derived from a single symmetric linker to make interpenetrated coordination polymers must be explained. Here network topology analysis provides insight. Regular polyhedra are convex polyhedrons that have identical faces derived from equivalent regular polygons and identical vertices assembled from a single type of polygon. There are exactly five such solids: the cube, tetrahedron, octahedron, dodecahedron, and icosahedron.[27,28] On the other hand, semiregular solids (13 in all) are convex polyhedra that have two or more different types of regular polygons as faces, with sides all of the same length and arranged in the same way about each vertex.[28,29] Such network substructures readily arise from high symmetry linkers coordinating to symmetric metal clusters because there exists only a single distance between coordinating groups. In our approach, reduced symmetry linkers will generally not form cage structures whose shapes are those of regular or semiregular polyhedra; a result of the nonuniformity of distances between coordinating groups. This will promote the formation of highly porous materials because the networks lack the appropriate symmetry for self-interpenetration.

We recently disclosed the utility of linker symmetry reduction with the report of University of Michigan Crystalline Material (UMCM)-150 which incorporates a C_{2v} symmetric linker, biphenyl-3,4′,5-tricarboxylate (**1**).[16] This was the first porous material derived from a linker containing only chemically inequivalent carboxylates with distinct coordination environments. Two types of metal clusters are formed upon coordination of **1** with copper, $Cu_2(CO_2R)_4$ paddlewheels and $Cu_3(CO_2R)_6$ trigonal prismatic clusters. The presence of the trinuclear Cu cluster in UMCM-150 is remarkable, considering it had not been previously formed in an MCP and because the paddlewheel is by far the most commonly formed metal cluster involving carboxylate coordination. Consequently, the structure of UMCM-150 is a non-interpenetrated [3,4,6]-connected network with a BET (Brunauer−Emmett−Teller) surface area of ∼3000 m^2/g. The topological complexity in UMCM-150 is attributed to the symmetry of linker **1** which drives the formation of a new network needed to fulfill the enthalpic requirements imposed by a unique linker geometry. However, with only one example, it is difficult to generalize as to the behavior of reduced symmetry linkers in the formation of coordination polymers. Here five examples of MCPs are presented to allow assessment of the general utility of this linker design strategy.

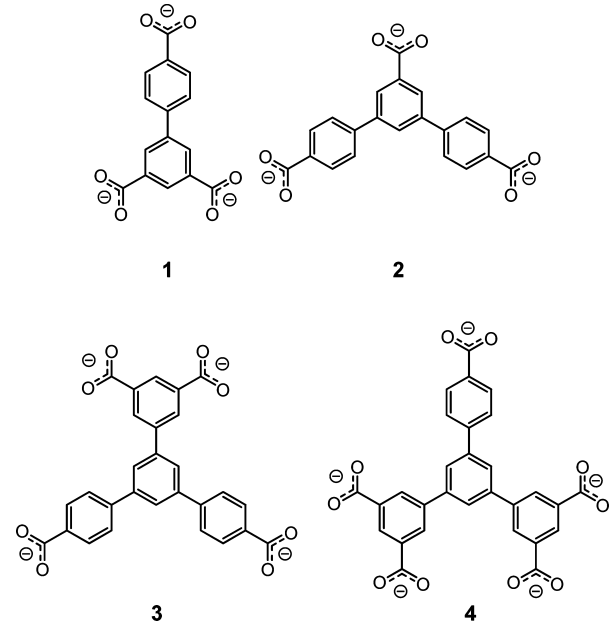

Experimental Section

All chemical reagents were obtained from commercial sources and, unless otherwise noted, were used as received.

Preparation of $H_3$2. Methyl-3,5-dibromobenzoate (1.00 g, 3.66 mmol), methyl-4-carboxyphenylboronic acid[30] (1.38 g, 7.69 mmol) and K_3PO_4 (4.66 g, 22.0 mmol) were combined in 1,4-dioxane (40

(21) Shekhah, O.; Wang, H.; Paradinas, M.; Ocal, C.; Schupbach, B.; Terfort, A.; Zacher, D.; Fischer, R. A.; Woll, C. *Nat. Mater.* **2009**, *8*, 481–484.
(22) Farha, O. K.; Malliakas, C. D.; Kanatzidis, M. G.; Hupp, J. T. *J. Am. Chem. Soc.* **2010**, *132*, 950–952.
(23) He, H.; Yuan, D.; Ma, H.; Sun, D.; Zhang, G.; Zhou, H.-C. *Inorg. Chem.* **2010**, *49*, 7605–7607.
(24) Zhang, J.; Wojtas, L.; Larsen, R. W.; Eddaoudi, M.; Zaworotko, M. J. *J. Am. Chem. Soc.* **2009**, *131*, 17040–17041.

mL), and the solution was sparged with N_2 gas for 30 min. $Pd(PPh_3)_4$ (0.130 g, 0.112 mmol) was added, and the suspension was stirred under N_2 for 20 h at 100 °C in a pressure vessel. After cooling, H_2O (~100 mL) was added, and a white solid precipitated. The coupled product was collected by filtration and purified through column chromatography on silica gel using CH_2Cl_2 as the eluent. The material was hydrolyzed in a solution of KOH (1.5 M) in dioxane/H_2O (4:1, 20 mL) by heating at reflux for 18 h. The solvent was evaporated, and the residue was dissolved in water. The solution was acidified (pH ≈ 2) by addition of conc HCl. The resulting white precipitate was collected by centrifugation, washed by resuspending in water, and then recollected by centrifugation. After multiple washing cycles the solid was dried under vacuum (0.92 g, 69%). Mp > 300 °C; ^{1}H NMR (500 MHz, $CDCl_3$): δ 13.14 (br, 3H), 8.29 (d, 2H, J = 1.6 Hz), 8.26 (t, 1H, 1.6 Hz, 8.06 (m, 4H), 7.97, (m, 4H); ^{13}C NMR (125 MHz, $CDCl_3$): δ 167.1, 166.9, 143.1, 140.4, 132.5, 130.2, 130.0, 129.9, 127.3 HRMS (EI) (*m*/*z*) calcd (found) for $C_{21}H_{14}O_6$: 362.0790 (362.0805).

Preparation of Intermediates for $H_4$3 and $H_5$4. 1,3,5-Tribromobenzene (3.32 g, 10.5 mmol), methyl-4-carboxyphenylboronic acid (4.17 g, 23.2 mmol,) and K_3PO_4 (13.4 g, 63.2 mmol) were combined in 1,4-dioxane (125 mL) and sparged with N_2 gas for 30 min. $Pd(PPh_3)_4$ (0.300 g, 0.260 mmol) was added, and the suspension was stirred under N_2 for 20 h at 100 °C in a pressure vessel. After cooling, H_2O (~1 L) was added, and a white solid precipitated. The precipitate was dissolved in CH_2Cl_2 and dried over Na_2SO_4. The monocoupled and dicoupled esters were isolated using column chromatography on silica gel with CH_2Cl_2 and hexanes (75% CH_2Cl_2/25% hexanes to 100% CH_2Cl_2) as the eluent. Dimethyl 5′-bromo-[1,1′:3′,1″-terphenyl]-4,4″-dicarboxylate: (3.12 g, 31.6%) ^{1}H NMR (500 MHz, $CDCl_3$): δ 8.14 (m, 4H), 7.77 (d, 2H, J = 1.6 Hz), 7.75 (t, 1H, J = 1.6 Hz), 7.68 (m, 4H), 3.96 (s, 6H); ^{13}C NMR (125 MHz, $CDCl_3$): δ 166.7, 143.8, 142.7, 130.3, 129.8, 129.7, 127.2, 125.0, 123.6, 52.2. Methyl 3′,5′-dibromo-[1,1′-biphenyl]-4-carboxylate: (1.61 g, 43.5%) ^{1}H NMR (500 MHz, $CDCl_3$): δ 8.12 (m, 2H), 7.68 (s, 3H), 7.60 (m, 2H), 3.95 (s, 3H); ^{13}C NMR (125 MHz, $CDCl_3$): δ 166.7, 143.5, 142.6, 133.4, 130.3, 130.0, 129.2, 127.1, 123.4, 52.3.

Preparation of $H_4$3. Dimethyl 5′-bromo-[1,1′:3′,1″-terphenyl]-4,4″-dicarboxylate (0.69 g, 1.6 mmol), dimethyl isophthalate-5-pinacolboronate[31] (0.63 g, 1.96 mmol) and K_3PO_4 (1.0 g, 4.8 mmol) were combined in 1,4-dioxane/H_2O (9:1, 15 mL) and sparged with N_2 gas for 30 min. $Pd(PPh_3)_4$ (0.037 g, 0.036 mmol) was added, and the suspension was stirred under N_2 for 16 h at 100 °C in a pressure vessel. After cooling the solvent was evaporated, and the crude product was taken up in CH_2Cl_2. The solution was cooled (−80 °C), and the precipitate was collected by cold filtration and dried. The material was hydrolyzed in a solution of KOH (1 M) in dioxane/H_2O (2:1, 20 mL) by heating at reflux for 18 h. The solvent was evaporated, and the residue was dissolved in water. The solution was acidified (pH ≈ 2) through addition of conc HCl. The resulting white precipitate was collected by centrifugation, washed by resuspending in water, and then recollected by centrifugation. After multiple washing cycles the solid was dried under vacuum (0.54 g, 69%). ^{1}H NMR (500 MHz, DMSO-d_6): δ 13.24 (br, 4H), 8.56 (d, 2H, J = 1.6 Hz), 8.52 (t, 1H, J = 1.5 Hz), 8.10 (t, 1H, J = 1.6 Hz), 8.08 (d, 2H, J = 1.6 Hz), 8.04 (s, 3H). ^{13}C NMR (100 MHz, $CDCl_3$): δ (167.1, 166.5, 143.7, 140.8, 140.8, 140.3, 132.2, 131.9, 130.0, 129.9, 127.5, 125.6. HRMS (EI) (*m*/*z*) calcd (found) for $C_{28}H_{18}O_8$: 482.1002 (482.1007).

Preparation of $H_5$4. Dimethyl 5′-bromo-[1,1′:3′,1″-terphenyl]-4,4″-dicarboxylate (1.00 g, 2.70 mmol), dimethyl isophthalate-5-pinacolboronate (2.18 g, 6.49 mmol) and K_3PO_4 (3.45 g, 16.2 mmol) were combined in 1,4-dioxane/H_2O (9:1, 35 mL) and sparged with N_2 gas for 30 min. $Pd(PPh_3)_4$ (0.125 g, 0.108 mmol) was added, and the suspension was stirred under N_2 for 8 h at 100 °C in a pressure vessel. After cooling the solvent was evaporated, and the crude product was taken up in CH_2Cl_2. The solution was cooled (−80 °C), and the precipitate was collected by cold filtration and dried. The material was hydrolyzed in a solution of KOH (1 M) in dioxane/H_2O (2:1, 25 mL) by heating at reflux for 18 h. The solvent was evaporated, and the residue was dissolved in water. The solution was acidified (pH ≈ 2) through addition of conc M HCl. The resulting white precipitate was collected by centrifugation, washed by resuspending in water, and then recollected by centrifugation. After multiple washing cycles the solid was dried under vacuum (0.423 g, 31%). mp >300 °C ^{1}H NMR (500 MHz, DMSO-d_6): δ 13.15 (br, 5H), 8.54 (d, 4H, J = 1.6 Hz), 8.49 (t, 2H, J = 1.6 Hz), 8.04 (m, 7H), ^{13}C NMR (125 MHz, DMSO-d_6): δ 167.2, 167.0, 143.6, 140.9, 140.7, 140.2, 133.4, 131.3, 130.4, 129.9, 129.3, 127.4, 125.5, 125.3 HRMS (EI) (*m*/*z*) calcd (found) for $C_{29}H_{18}O_{10}$ [M − H]$^-$: 525.0827 (525.0822).

Preparation of UMCM-151 [$Cu_2(C_{21}H_{11}O_6)_{1.33}$]. Linker H_2**2** (0.050 g, 0.14 mmol) was added to a solution of DMF/dioxane/H_2O (4:1:1, 10 mL) in a 20-mL scintillation vial. To this mixture was added $Cu(NO_3)_2 \cdot 2.5H_2O$ (0.096 g, 0.41 mmol), and the contents were sonicated until dissolved and then heated at 85 °C. After 12 h, the mother liquor was decanted and replaced with fresh DMF/dioxane/H_2O (4:1:1). The blue crystals were exchanged twice in DMF and five times in acetone. The material was dried under vacuum at room temperature for 4 h in which time the crystals turned green. The yield of the reaction based upon the weight of the solvent-free material is 80% based upon H_3**2**. Anal. Calcd (Found) for $[Cu_2(C_{21}H_{11}O_6)(H_2O)_5]$: C, 52.39 (51.96) H, 2.89 (2.50).

Preparation of UMCM-152 [$Cu_2(C_{28}H_{14}O_8)$]. Linker H_4**3** (0.050 g, 0.10 mmol) was added to a solution of 0.005 M HCl in DMF/dioxane/H_2O (4:1:1, 10 mL) in a 20-mL scintillation vial. To this mixture, $Cu(NO_3)_2 \cdot 2.5H_2O$ (0.096 g, 0.41 mmol) was added, and the contents were sonicated until dissolved and then heated at 85 °C. After 12 h, the mother liquor was decanted and replaced with fresh DMF/dioxane/H_2O (4:1:1). Blue block-like crystals were washed twice with DMF and five times with acetone. Solvent was removed under vacuum for 4 h and further dried at 100 °C for 18 h to yield a dark-purple material. The yield of the reaction based upon the weight of the solvent-free material is 82% based upon H_4**3**. Anal. Calcd (Found) for $[Cu_2(C_{28}H_{14}O_8)(H_2O)_{1.5}]$: C, 53.17 (52.89) H, 2.71 (2.28).

Preparation of UMCM-153 [$Cu_2(C_{28}H_{14}O_8)$]. Linker H_4**3** (0.050 g, 0.10 mmol) was added to a solution of NMP/dioxane/H_2O (4:1:1, 10 mL) in a 20-mL scintillation vial. To this mixture, $Cu(NO_3)_2 \cdot 2.5H_2O$ (0.096 g, 0.41 mmol) was added, and the contents were sonicated until dissolved and then heated at 85 °C. After 24 h, the mother liquor was decanted and replaced with fresh NMP/dioxane/H_2O (4:1:1). Blue blade-like crystals were washed twice with DMF and five times with acetone. Solvent was removed under vacuum for 4 h and further dried at 100 °C for 18 h to yield a dark-purple material. The yield of the reaction based upon the weight of the solvent-free material is 55% based upon H_4**3**. Anal. Calcd (Found) for $[Cu_2(C_{28}H_{14}O_8)(H_2O)_{1.5}]$: C, 53.17 (53.37) H, 2.71 (2.50).

Preparation of UMCM-154 [$Zn_2(C_{29}H_{14}O_{10})$]. Linker H_5**4** (0.050 g, 0.095 mmol) was added to DMF (10 mL) in a 20-mL scintillation vial. To this mixture, $Zn(NO_3)_2 \cdot 6H_2O$ (0.14 g, 0.47 mmol) was added, and the contents were sonicated until dissolved and heated at 85 °C. After 24 h the mother liquor was decanted

(25) Hong, S.; Oh, M.; Park, M.; Yoon, J. W.; Chang, J. S.; Lah, M. S. *Chem Commun.* **2009**, 5397–5399.
(26) Eddaoudi, M.; Nouar, F.; Eubank, J. F.; Wojtas, L.; Bousquet, T.; Zaworotko, M. Supramolecular assemblies and building blocks. U.S. Pat. Appl. 20090143596 A1, filed November 17th 2008.
(27) Weisstein, E. W. Platonic Solid. MathWorld: A Wolfram Web Resource. http://mathworld.wolfram.com/PlatonicSolid.html.
(28) Wells, A. F.; *The Third Dimension in Chemistry*; Clarendon Press: Oxford, London, 1956, p 143.
(29) Weisstein, E. W. Archimedean Solid. MathWorld: A Wolfram Web Resource. http://mathworld.wolfram.com/ArchimedeanSolid.html.
(30) Percec, V.; Won, B. C.; Peterca, M.; Heiney, P. A. *J. Am. Chem. Soc.* **2007**, *129*, 11265–11278.
(31) Natera, J.; Otero, L.; Sereno, L.; Fungo, F.; Wang, N.-S.; Tsai, Y.-M.; Hwu, T.-Y.; Wong, K.-T. *Macromolecules* **2007**, *40*, 4456–4463.

and replaced with fresh DMF. Crystals were washed twice with DMF and five times with CH_2Cl_2 to yield colorless polygons. The solvent was removed under vacuum for 6 h, and the yield of the reaction based upon the weight of $[Zn_2(C_{29}H_{14}O_{10})(C_3H_6NO)(H_2O)_5]$ is 87% based upon H_5**4**. Anal. Calcd (Found) for $[Zn_2(C_{29}H_{14}O_{10})(C_3H_6NO)(H_2O)_5]$: C, 47.14 (47.45), H, 3.71 (3.59), N, 1.72 (2.26).

Gas Sorption. Nitrogen adsorption/desorption isotherms were measured volumetrically at 77 K in the range $1.00 \times 10^{-3} \leq P/P_o \leq 1.00$ with an Autosorb-1C outfitted with the micropore option by Quantachrome Instruments (Boynton Beach, Florida U.S.A.), running version 1.2 of the ASWin software package. Ultrahigh purity He (99.999%, for void volume determination) and N_2 (99.999%) were purchased from Cryogenic Gases and used as received. MCPs exchanged with acetone were charged into a sample cell and dried under vacuum (<0.1 mTorr) at 100 °C. The resulting mass of dried material in the cell was ~10 mg. The specific surface areas were determined using either the BET or the Langmuir equation.

Argon sorption experiments were performed at 87 K in the range $1.00 \times 10^{-4} \leq P/P_o \leq 1.00$ with ultrahigh purity Ar (99.999%) purchased from Cryogenic Gases. Pore size distributions were calculated using the nonlocal density functional theory (NLDFT) zeolite/silica equilibrium transition kernel for Ar adsorption at 87 K based on a cylindrical pore model as implemented in version 1.2 of the ASWin software package.

Volumetric hydrogen adsorption measurements were performed on ~400 mg samples using an automated volumetric Sieverts' apparatus (PCT-Pro 2000 from Hy-Energy LLC) over the 0−60 bar range. The excess hydrogen adsorption isotherms were calculated from successive gas expansions by adding the differences between the amounts of gas depleted from the reference cell and that occupying the sample cell after each expansion. Dead space volumes were determined at room temperature using helium gas as a negligibly adsorbing gas. Ultrahigh purity hydrogen and helium (99.999% purity) obtained from Airgas Inc. were used for all measurements.

Crystal Structure Determination. Single crystals suitable for X-ray structure determination were selected under a microscope and mounted in MiTiGen micromounts or on Nylon loops with Paratone N hydrocarbon oil and placed in a stream of cold nitrogen from an Oxford Cryosystems Cryostream Plus cooler for low-temperature data collection. For the room temperature collection, suitable crystals were glued to the end of a thin glass capillary. Intensity data were collected on a three circle (quarter χ-arm) Rigaku R-Axis Spider diffractometer (460 mm × 256 mm curved imaging plate detector with graphite monochromated Cu Kα radiation (λ = 1.54187 Å)). Initial ω scans of each sample were performed to determine preliminary unit cell parameters and to allow the selection of image widths for data collection. For all cases oscillation images were collected using widths of 2.0−2.5° in ω. Data were collected using the d*TREK package in the CrystalClear software suite[32] to obtain ω scans for χ at 0° and 54°. Using the FS_PROCESS[33] package in CrystalClear, the raw intensity data were then reduced to F^2 values with corrections for Lorentz, and polarization effects. Decay of the crystals during data collection was negligible. An empirical absorption correction was applied as implemented by FS_PROCESS. The structures were solved within the CrystalStructure[34] package by direct methods and refined against all data.[35] Hydrogen atoms were placed at calculated positions (C−H = 0.93 Å) using a riding model with isotropic displacement parameters scaled by the U_{eq} of the attached carbon atom. Thermal parameters for all non-hydrogen atoms were refined anisotropically. In structures with voids, attempts to locate and model the highly disordered solvent molecules in the voids were unsuccessful. Therefore, the SQUEEZE routine of PLATON[36] was used to remove the diffraction contribution from these solvents to produce a set of solvent-free diffraction intensities.

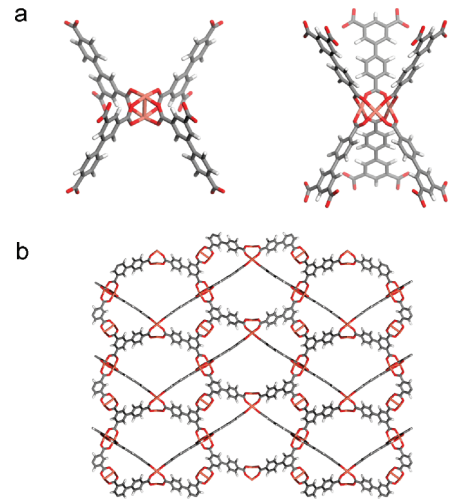

Figure 2. (a) View of the $Cu_2(CO_2R)_4$ paddlewheel and $Cu_3(CO_2R)_6$ trigonal prismatic clusters present in UMCM-150. (b) View of the network connectivity along the *a*-axis of UMCM-150.

Results and Discussion

Among the important findings that arose from the synthesis of UMCM-150 was an uncommon structural motif. In addition to the ubiquitous $Cu_2(CO_2R)_4$ paddlewheel, a trinuclear cluster with the formula $Cu_3(CO_2R)_6$ was found (Figure 2a). In this structure, all paddlewheels arise from isophthalate coordination connected through corrugated sheets joined by coordination of *p*-benzoate groups forming trinuclear clusters. Each $Cu_3(CO_2R)_6$ cluster forms a trigonal prismatic geometry orienting six *p*-benzoate groups along the *c*-axis (Figure 2b). There are three times as many paddlewheels as trigonal prismatic clusters.

Although the $Cu_3(CO_2R)_6$ cluster was unprecedented in coordination polymers, the formation can be rationalized by the 1:2 ratio of symmetry inequivalent carboxylates of **1** dictating that one type of paddlewheel, having a capacity for four carboxylate groups, cannot exclusively form within a structure. Consequently, if a paddlewheel is formed, another metal cluster (symmetry inequivalent paddlewheel or different cluster geometry) must also be present. In this case, segregation occurs among the chemically distinct carboxylates with isophthate carboxylates assembling into Cu paddlewheels and *p*-benzoate groups forming a new mode of assembly, a $Cu_3(CO_2R)_6$ cluster.

Extension of **1** through the addition of a benzene ring leads to linker **2**, and assembly of this linker with Cu produces UMCM-151. This structure does not share the same net as UMCM-150 even though **2** possesses the same number of carboxylates and C_{2v} symmetry as linker **1**. Monocarboxylated rings are present with *p*-benzoate groups attached to a central benzene ring possessing a carboxylate in the 5-position (herein referred to as *m*-carboxylate), thus changing the distance between nodes and angles of extension between coordinating groups of the linker and allowing a new structure to form. Similar to the case with linker **1**, the 1:2 ratio of carboxylate

(32) *CrystalClear 2.0*; Rigaku and Rigaku/MSC: The Woodlands, TX, 2009.
(33) Higashi, T. *Program for Absorption Correction*; Rigaku Corporation: Tokyo, Japan, 1995.
(34) *CrystalStructure 3.8.1: Single Crystal Structure Analysis Software*; Rigaku and Rigaku/MSC: The Woodlands, TX, 2007.
(35) Sheldrick, G. M. *SHELXS '97 and SHELXL '97, Programs for Crystal Structure Analysis*; University of Göttingen, Göttingen, Germany, 1997.
(36) Spek, A. L. *PLATON, A Multipurpose Crystallographic Tool*; Utrecht University: Utrecht, The Netherlands, 2005.

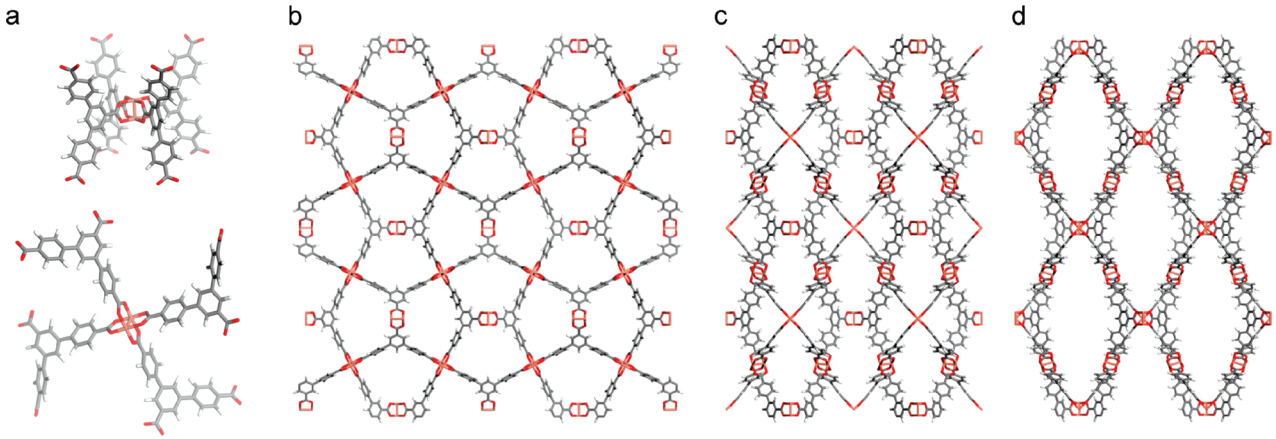

Figure 3. (a) Separate Cu paddlewheels are formed through the coordination of four *m*-carboxylate groups and four *p*-benzoate groups in UMCM-151. (b) View of the pentagonal channels along the *a*-axis. (c) View along the *b*-axis in UMCM-151. (d) View along the *c*-axis featuring 3-nm oblong-shaped channels.

types in **2** prevents a single kind of Cu paddlewheel cluster from forming. Segregation based upon carboxylate symmetry is also observed; however, in the case of UMCM-151, two different paddlewheels are present, with *p*-benzoate groups forming one type of paddlewheel and *m*-carboxylate groups of **2** forming a separate paddlewheel (Figure 3a). There are twice as many paddlewheels based upon *p*-benzoate coordination as *m*-carboxylate coordination in order to satisfy the stoichiometry of linker **2**.

UMCM-151 consists of a non-interpenetrated open-pore network crystallizing in the space group *Immm*. A view along the *a*-axis reveals pentagonal-shaped channels with dimensions, accounting for van der Waals radii, of 11.4 Å × 9.6 Å formed through the connection of three *p*-benzoate groups and two *m*-carboxylate groups coordinated through a Cu-paddlewheel (Figure 3b). These are intersected by another set of pentagonal channels (11.3 Å × 6.9 Å) defined by four *m*-carboxylate units and four *p*-benzoate groups coordinated with four Cu clusters along the *b*-axis (Figure 3c). The largest channels within UMCM-151 are oblong with pore dimensions of 28.4 Å × 11.0 Å spanning the *c*-axis (Figure 3d).

Attempts to activate UMCM-151 by heating under reduced pressure led to surface areas much lower than theoretical values predicted by the LiMe ratio surface area analysis[37] (4791 m^2/g) and geometric accessible surface area method[38] (4493 m^2/g). Examination of the PXRD pattern after solvent removal indicates significant loss of crystallinity consistent with structural collapse. The 3-nm channels within UMCM-151 may ultimately be responsible for this collapse, suggesting that three carboxylate groups cannot provide enough junction points for the *m*-terphenyl linker, **2**, to coordinate with Cu paddlewheels in a stable conformation.

In considering how to overcome the problem of low structural rigidity in UMCM-151, inspiration is derived from isophthalate-based MCPs and especially those possessing a ratio of benzene rings to carboxylates of 1 or greater.[7,9,12,15,39] To implement this design while maintaining reduced symmetry, **3** was considered as a C_{2v} tetracarboxylate precursor. This ligand can be conceptually derived from 1,3,5-tris(4-carboxyphenyl)benzene by replacing one phenyl carboxylate with an isophthalate group. Gratifyingly, this ligand led to two non-interpenetrated coordination polymers that both maintain porosity.

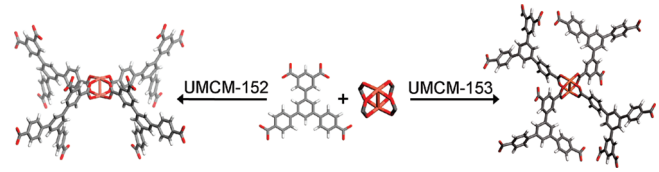

Figure 4. Coordination of linker **3** with Cu to form paddlewheels. Adjacent coordination of two equivalent carboxylates leads to the formation of UMCM-152, whereas an alternating pattern of carboxylate types leads to UMCM-153.

Solvothermal synthesis in a solution of 4:1:1 DMF/dioxane/H_2O with H_4-**3** and $Cu_2(NO_3)_2 \cdot 2.5H_2O$ affords a mixture of blue block-shaped crystals of UMCM-152 and blue blade-like crystals of UMCM-153. UMCM-152 can be formed as a pure phase through the addition of 0.005 M HCl to the reaction solution, and UMCM-153 can be produced pure from a mixture of 4:1:1 *N*-methyl-2-pyrrolidone (NMP)/dioxane/H_2O.

A key distinction between UMCM-152 and UMCM-153 is the pattern of carboxylate coordination to form Cu paddlewheels. Linker **3** contains two pairs of chemically equivalent carboxylates: an isophthalate group and two *p*-benzoate units. Therefore, carboxylate segregation may occur, as in the cases of UMCM-150 and UMCM-151, or chemically inequivalent carboxylates may blend to form one or more types of mixed carboxylate paddlewheels. Single-crystal X-ray analysis reveals that both materials feature one unique paddlewheel containing two carboxylates of each type; however, the arrangement of these groups is very different. In UMCM-152, two isophthalate carboxylates assemble in adjacent positions joined by two adjacent *p*-benzoate groups, whereas coordination of chemically inequivalent units alternates in UMCM-153 (Figure 4). Consequently, the differences in paddlewheel coordination prompt the formation of two distinct structures, but because they have the same building block components, UMCM-152 and UMCM-153 are polymorphic frameworks.[40] Although several examples

(37) Schnobrich, J. K.; Koh, K.; Sura, K. N.; Matzger, A. J. *Langmuir* **2010**, *26*, 5808–5814.
(38) Düren, T.; Millange, F.; Férey, G.; Walton, K. S.; Snurr, R. Q. *J. Phys. Chem. C* **2007**, *111*, 15350–15356.
(39) Lin, X.; Jia, J. H.; Zhao, X. B.; Thomas, K. M.; Blake, A. J.; Walker, G. S.; Champness, N. R.; Hubberstey, P.; Schröder, M. *Angew. Chem., Int. Ed.* **2006**, *45*, 7358–7364.
(40) Caskey, S. R.; Wong-Foy, A. G.; Matzger, A. J. *Inorg. Chem.* **2008**, *47*, 7751–7756.

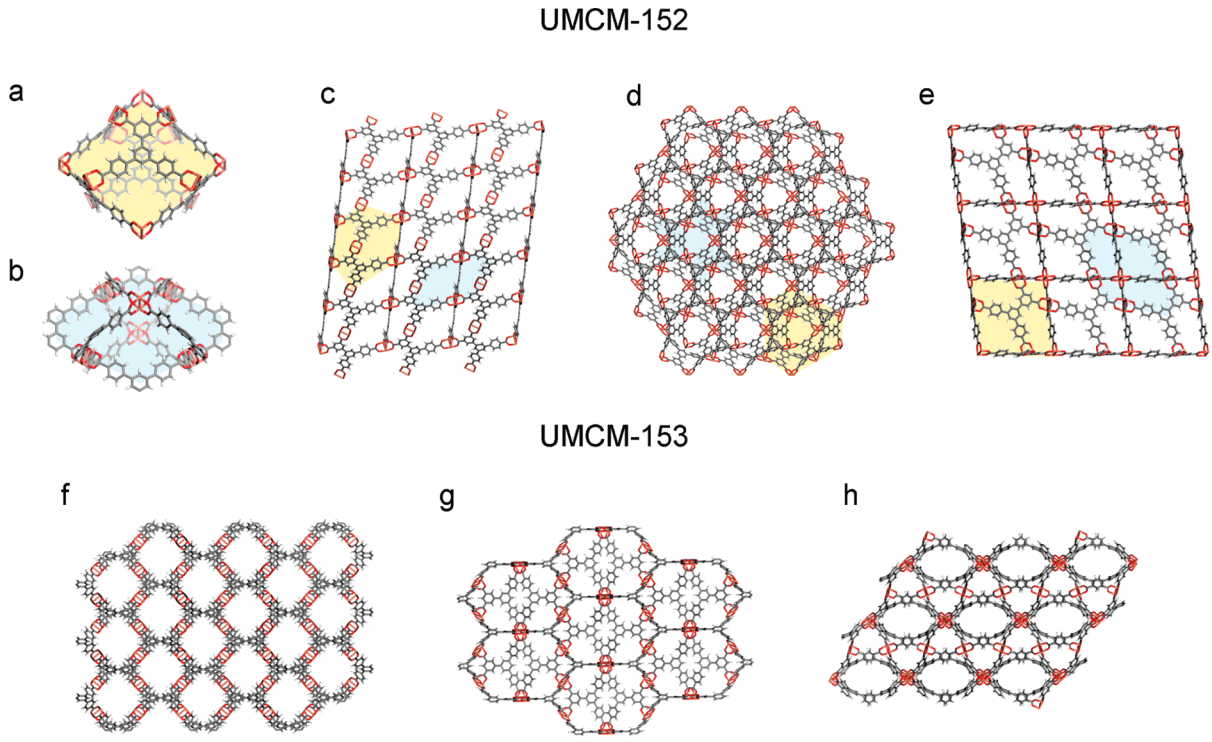

Figure 5. (a) One cage in UMCM-152 is defined by the faces of six linkers and twelve Cu-paddlewheels to form a distorted hexagonal bipyramid. (b) Another cage is formed by the edges of twelve linkers and six Cu-paddlewheels. (c) View along the *a*-axis. (d) View along the *c*-axis. (e) View of the 302 plane of UMCM-152. (f) View along the *a*-axis of UMCM-153 featuring channels aligned with coordinatively unsaturated metal sites. (g) View of the channel walls of the 470 plane. (h) Intersecting elliptical channels in the 104 plane in UMCM-153.

have been generated from fully symmetric linkers,[17,40−43] reduced symmetry linkers offer significantly more assembly modes because both linker orientation and inequivalent carboxylate coordination can produce diverse networks from the same linker and metal cluster.

The structure of UMCM-152 belongs to the space group *R*3*m* and consists of two types of alternatively stacked cages. The first cage is defined by the faces of six linker molecules and twelve metal clusters to form a distorted hexagonal bipyramid with pore apertures of approximately 7.5 Å (Figure 5a). Apical positions are occupied by a set of three isophthalate groups coordinated to three paddlewheels with small cylindrical pores of 4.1 Å and a set of six *p*-benzoates coordinating to three paddlewheels with a larger pore size of 10.6 Å. Coordination in the equatorial region of this cage consists of an alternating pattern of two *p*-benzoate groups and isophthalates joined to six paddlewheel clusters. The inner diameter of this cage is approximately 18.6 Å. A second cage is formed from the edges of twelve linkers and six Cu paddlewheels (Figure 5b). Apical positions and pore apertures are shared with the first cage, and the inner diameter of this cage is 16.9 Å. A view down the *a*-axis and *c*-axis are provided (respectively Figure 5c and Figure 5d) as well as a view of the 302 plane (Figure 5e) highlighting the two cages present in UMCM-152.

UMCM-153 crystallizes in the space group *Fddd*. Hexagonal channels align along the *a*-axis, producing cylindrical pores of 8.7 Å (Figure 5f). These channels are formed through the stacking of cages defined by the faces of four whole linkers and the edges of four isophthalate groups and two sets of *m*-terphenyl linked *p*-benzoate fragments joined by twelve Cu paddlewheels. The inside of each cage possesses four coordinatively unsaturated metal sites which are oriented toward the center of the hexagonal channel. A view of the 470 plane (Figure 5g) displays the channel walls defined by the faces of linker **3.** The connection of two isophthalate groups and four *p*-benzoate groups produce an intersecting channel with dimensions of 15.0 Å × 4.4 Å (Figure 5h).

The surface areas of UMCM-152 and UMCM-153 were determined from N_2 adsorption isotherms at 77 K, revealing that UMCM-152 has a BET surface area of 3480 m^2/g (Langmuir 3850 m^2/g) and UMCM-153 has a value of 3370 m^2/g (Langmuir 3730 m^2/g) (Figure 6a), and these values are in good agreement with geometric accessible surface area predictions. Pore size distributions were determined with NLDFT calculations from Ar adsorption isotherms at 87 K, corresponding to pore sizes of 8−10 and 10−11.5 Å for UMCM-152 and of 7−10.5 and 10.5−11.5 Å for UMCM-153; these ranges are consistent with crystallographic data. A small distribution of 40.5−46.0 Å is also found in UMCM-153, signaling either a deficiency in applying the NLDFT model to the irregular pore shape of UMCM-153 or defects within the material as has previously been found in MOF-5.[44] The excess hydrogen uptake for UMCM-152 at 77 K and 25 bar is 5.7%. This value is similar to the capacity of UMCM-153, 5.8% at 77 K and 29 bar, indicating that UMCM-152 and UMCM-153

(41) Wang, X. S.; Ma, S. Q.; Forster, P. M.; Yuan, D. Q.; Eckert, J.; López, J. J.; Murphy, B. J.; Parise, J. B.; Zhou, H.-C. *Angew. Chem., Int. Ed.* **2008**, *47*, 7263–7266.
(42) Sun, D. F.; Ke, Y. X.; Mattox, T. M.; Ooro, B. A.; Zhou, H.-C. *Chem. Commun.* **2005**, 5447–5449.
(43) Sun, D.; Ma, S.; Simmons, J. M.; Li, J.-R.; Yuan, D.; Zhou, H.-C. *Chem. Commun.* **2010**, *46*, 1329–1331.
(44) Liu, M.; Wong-Foy, A. G.; Vallery, R. S.; Frieze, W. E.; Schnobrich, J. K.; Gidley, D. W.; Matzger, A. J. *Adv. Mater.* **2010**, *22*, 1598–1601.

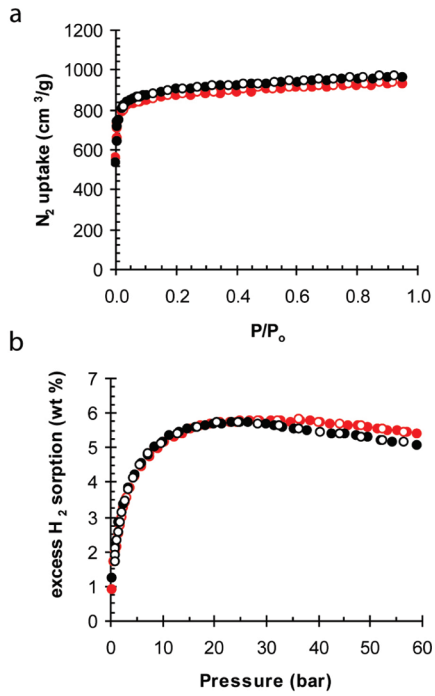

Figure 6. (a) Nitrogen sorption isotherms at 77 K for UMCM-152 (black) and UMCM-153 (red) (b) High-pressure excess hydrogen isotherms at 77 K (closed markers: adsorption, open markers: desorption).

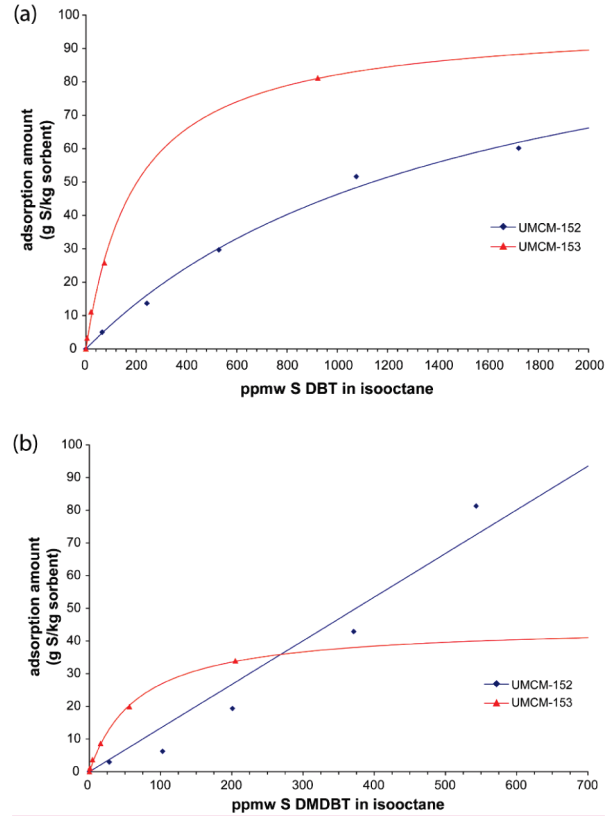

Figure 7. Adsorption isotherms for (a) DBT and (b) DMDBT for UMCM-152 (blue) and UMCM-153 (red). The curves represent a fit to the Langmuir equation and are intended as guides to the eye.

have similar gas sorption properties despite differences in pore shape (Figure 6b). Considering identical linker and metal cluster components and similarities in surface area, differences in sorption properties in UMCM-152 and UMCM-153 might be expected to arise when guest size more closely matches pore dimensions; this hypothesis motivated us to examine larger guest inclusion of the sort that can be realized in liquids.[45]

Recently MCPs have been shown to remove organosulfur compounds from model fuels and diesel representing an efficient method for reaching new sulfur level targets in diesel and gasoline set by the U.S. Department of Transportation.[46,47] UMCM-152 and UMCM-153, having the same building block units and nearly identical surface areas, offer an opportunity to study the effect of framework structure in the absence of variation in linker or metal cluster. Adsorption isotherms were measured out to 2000 ppmw S for dibenzothiophene (DBT) (Figure 7a) and to 600 ppmw S for 4,6-dimethyldibenzothiophene (DMDBT) (Figure 7b) in isooctane. UMCM-152 and UMCM-153 exhibit tremendous capacities for DBT and DMDBT: DBT capacities (g S/kg MCP, 1500 ppmw S) are 59 and 89 and DMDBT capacities (g S/kg MCP, 600 ppmw S) are 82 and 40, respectively. These values exceed considerably those of published MCPs. The dramatic differences in capacity of DBT and DMDBT in UMCM-152 and UMCM-153 provide indisputable evidence that liquid phase adsorption is not dependent on surface area or linker or metal cluster identity. Moreover, this constitutes a unique case where the equilibrium adsorption capacity for large molecules in the liquid phase can be directly credited to effects of pore size and shape[46,48] UMCM-153 adsorbs more DBT than UMCM-152 over the entire concentration range examined likely due to a better fit of DBT in the pores of UMCM-153. At low DMDBT concentrations UMCM-153 again outperforms UMCM-152. However, at higher concentrations where the uptake of UMCM-153 begins to level off, the UMCM-152 isotherm continues to rise, leading to higher adsorption capacities at high DMDBT concentration than for UMCM-153. It is postulated that at higher DMDBT concentrations the larger DMDBT molecules begin to block further uptake in the smaller UMCM-153 pores. In contrast, the larger pores of UMCM-152 can readily accommodate the DMDBT molecule in such a way such that the pore apertures are not blocked for further adsorption.

Further increasing the number of carboxylates around the triphenylbenzene core while maintaining C_{2v} symmetry leads to linker **4**. Statistical analysis reveals that the 4:1 ratio of chemically equivalent carboxylates cannot form only one type of $M_2(CO_2R)_4$ paddlewheel; however, segregation involving *p*-benzoate groups coordinating to form one type of paddlewheel with isophthalates forming another paddlewheel or a series of mixed carboxylate paddlewheels may be plausible. Attempts to form a coordination polymer with Cu have thus far failed; however, Zn coordinates with **4** to form an MCP termed UMCM-154.

The metal cluster present in UMCM-154 is uncommon, consisting of a three-bladed zinc paddlewheel with three

(45) Cychosz, K. A.; Ahmad, R.; Matzger, A. J. *Chem. Sci.* **2010**, *1*, 293–302.
(46) Cychosz, K. A.; Wong-Foy, A. G.; Matzger, A. J. *J. Am. Chem. Soc.* **2008**, *130*, 6938–6939.
(47) Cychosz, K. A.; Wong-Foy, A. G.; Matzger, A. J. *J. Am. Chem. Soc.* **2009**, *131*, 14538–14543.
(48) Vaidhyanathan, R.; Bradshaw, D.; Rebilly, J.-N.; Barrio, J. P.; Gould, J. A.; Berry, N. G.; Rosseinsky, M. J. *Angew. Chem., Int. Ed.* **2006**, *45*, 6495–6499.

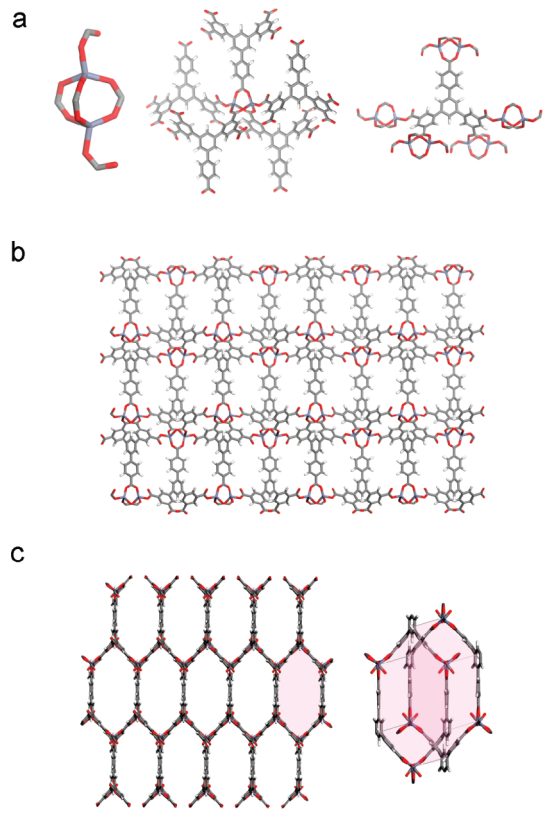

Figure 8. (a) Views of the three-bladed zinc paddlewheel metal cluster in UMCM-154. Each metal cluster coordinates to four isophthalate carboxylates and one *p*-benzoate group. Each linker contributes three equatorial "paddle" carboxylates and two axial coordinating carboxylates. (b) View along the *a*-axis. (c) View of hexagonal pores formed through the connection of three linkers and three Zn metal clusters.

carboxylates coordinated to two tetrahedral zinc ions and an additional two carboxylates coordinated to the axial positions. In this cluster, two isophthalate and one *p*-benzoate coordinate to form paddlewheels. The two remaining isophthalate carboxylates coordinate in the axial positions in a monodentate fashion (Figure 8a). Crystallographic evidence does not indicate the presence of a counterion, suggesting that the metal cluster is uncharged. To satisfy this condition, half of the axial carboxylate groups must exist in the protonated form, generating a metal cluster formula of $Zn_2(CO_2)_4(CO_2H)$. The coordination geometry of this metal cluster has only been formed in MCP systems where severe steric strain[49] or copolymerization[50] of linkers is present. In UMCM-154, the formation of this three-bladed metal cluster over other more common Zn clusters is attributed to the thermodynamic requirements imposed by linker **4** having five carboxylates in a 1:4 symmetry equivalent ratio.

UMCM-154 exists in the space group *C2/c* and derives from a [5,5]-net. Sheets of isophthalate groups coordinating to the metal clusters are connected by pillars of *p*-benzoate groups (Figure 8b). Hexagonal channels of 14.9 Å × 6.8 Å are defined by three linkers coordinating with three metal clusters that stack in alternating directions (Figure 8c). UMCM-154 does not maintain permanent porosity upon guest removal. Collapse is attributed to an unstable metal cluster incorporating two monodentate coordinating carboxylates.

Conclusion

To summarize, reduced symmetry linkers offer a largely unexploited approach to the synthesis of high-performance coordination polymers. They can drive new modes of assembly as illustrated by UMCM-150 and UMCM-154, and even common metal clusters are susceptible to creating different networks due to supramolecular isomerism imparted by varying coordination modes of chemically distinct carboxylates. Polymorphic frameworks UMCM-152 and UMCM-153 show nearly identical gas adsorption properties and dramatically different capacities for organosulfur compounds providing direct evidence that liquid-phase adsorption is dependent on pore size and shape rather than the typical pillars of sorption behavior (linker identity, metal cluster identity, and surface area) alone. In addition, the inherent complexity of vertex desymmetrization associated with coordinating chemically distinct carboxylates to a metal cluster leads to highly porous materials lacking interpenetration rendering them important building blocks in the synthesis of a new generation of porous materials.

Acknowledgment. This work was funded by General Motors.

Supporting Information Available: Crystallographic information files; linker synthetic scheme, thermogravimetric analysis, PXRD patterns, BET and Langmuir surface area data, Ar isotherms and pore-size distributions. This material is available free of charge via the Internet at http://pubs.acs.org.

JA107423K

(49) Vagin, S.; Ott, A.; Weiss, H. C.; Karbach, A.; Volkmer, D.; Rieger, B. *Eur. J. Inorg. Chem.* **2008**, 2601–2609.
(50) Hou, L.; Zhang, J. P.; Chen, X. M. *Cryst. Growth Des.* **2009**, *9*, 2415–2419.